ARCTIC OBSERVATIONS WITH THE UNIVERSITY OF WISCONSIN HIGH SPECTRAL RESOLUTION LIDAR

Edwin W. Eloranta, Igor A. Razenkov, Joesph P. Garcia

University of Wisconsin, 1225 W. Dayton St., Madison, WI, USA, E-mail:eloranta@lidar.ssec.wisc.edu

ABSTRACT

The University of Wisconsin Arctic High Spectral Resolution Lidar has provided nearly continuous data since its August 2005 deployment at Eureka, Canada (80N, 85W). A prior deployment to Barrow, Alaska(71N, 156W) provided data between August 24 and November 17 of 2004. Cloud properties derived from these data are presented.

1. INTRODUCTION

The University of Wisconsin Arctic High Spectral Resolution Lidar (HSRL) operates as a minimally-tended Internet appliance. An expanded transmitted beam and low pulse energy make the output beam eye safe. Using molecular scattering as a calibration reference, the HSRL provides absolutely calibrated profiles of backscatter cross section, optical depth and depolarization [2; 6; 7].

Between August 24 and November 17, 2004 the HSRL was deployed to Barrow, Alaska (71N, 156W) as part of the US Department of Energy Mixed-Phase Arctic Cloud Experiment (MPACE). Since August 1, 2005 the HSRL has operated in the high Arctic at Eureka, Canada (80N, 85W) as part of the US National Oceanic and Atmospheric Administration (NOAA) SEARCH program. SEARCH seeks to provide continuous measurements of Arctic surface radiation, clouds, aerosols and chemistry sufficient for detailed evaluation of interactive climate change processes in the lower atmosphere. The NOAA 35 GHz cloud radar [3] and the University of Idaho Polar Atmospheric Emitted Radiance Interferometer (PAERI) [1] are located with the HSRL (Fig. 1).

During the MPACE and SEARCH deployments the HSRL has been programmed to provide profiles with 7.5 m vertical and 2.5 second temporal resolution. Usable data begins at 150 m above the surface and extends to 30 km. Lidar and radar data are posted on our web site: http://lidar.ssec.wisc.edu. Lidar data from altitudes below 15 km are posted in real time while the higher altitude data is transfered at approximately monthly intervals. Radar data is recorded with 30 m vertical and 10 second temporal resolution. Radar data is available approximately one day after it is recorded. Quick-look images show all lidar and radar data from one month on a single web page. Images and netcdf download files

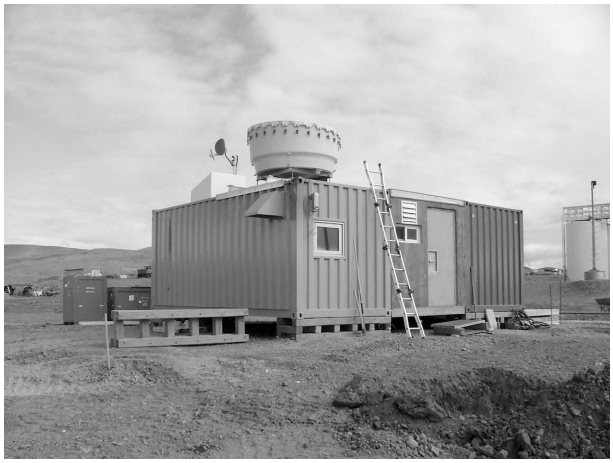

Figure 1. Two seatainers are joined together as shelter for the lidar, radar, and PAREI instruments. The radar antenna is on the near corner of the shelter and the lidar window is in the white box behind the radar antenna.

with user specified averaging, altitude ranges and time intervals can be generated via the web site. Lidar and radar data are presented with common grids allowing easy inter-comparison. Lidar data includes: depolarization, backscatter cross section, scattering cross section, and optical depth along with system housekeeping information. Radar data includes: reflectivity, backscatter cross section, Doppler velocity, and spectral width. Cloud particle effective diameter, number density, and liquid water content are computed using a combination of the lidar and radar data. These are computed following Donovan et at[4]. However, Donovan's iterative solution is not required because HSRL data is corrected for extinction, robustly calibrated, and the HSRL has a 45 micro-radian field-of-view that limits multiple scattering.

2. OPERATIONAL EXPERIENCE

The HSRL has provided nearly continuous data. Problems have included: 1) Shelter temperature excursions of ~ 10°C caused the main cavity of the laser to lose lock with the seed laser. The severity of this problem has been reduced by restricting flow through the shelter ventilation fan. 2) The Eureka station experiences frequent short interruptions of electrical power. Each time this

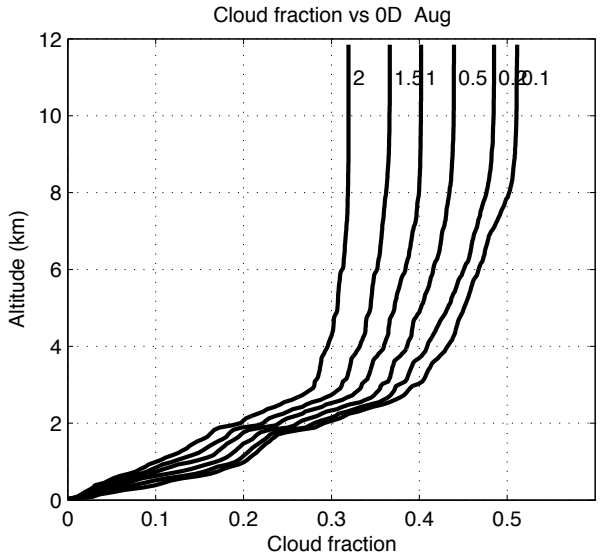

Figure 2. Cloud fraction as function of altitude for August, 2005 in Eureka. Curves show the fraction of the time that the atmosphere is clear up to a given altitude. Separate curves show the effect of changing the optical depth threshold that defines a cloud.

occurred several hours of down time occurred until we were able to contact Eureka and they were able to restart the laser. The duration of these interruptions has been reduced by installing a time-delay relay which automatically restarts the laser after a power interruption. 3) The optical alignment of the laser slowly degrades. This degrades the output power and the seeding efficiency of the laser. Maintenance visits at approximately 3-month intervals have been required to realign the laser. 4) Optical damage has occurred on the Brillouin frequency locking fiber and on the laser frequency doubling crystal. The Brillouin fiber has been repaired when the laser was realigned. The doubling crystal will need to be replaced on our next visit. The doubling crystal has lasted for more than 25,000 hours of operation. 5) The laser appears to exhibit small changes in the spatial/angular distribution of transmitted energy. This produces changes of $\sim .05$ in the optical depth measured by the lidar. It does not affect scattering cross section or depolarization measurements. 6) The laser seeding is somewhat erratic; at times, short periods of low seeding percentage reduce the useful output power and disturb the frequency lock of the laser to the iodine blocking filter. This problem is controlled by slightly changing the temperature of lidar enclosure or the laser cooling water. Temperature changes are accomplished via the Internet.

3. CLOUD OBSERVATIONS

Considerable uncertainty exists in current satellite derived Arctic cloud climatologies. Visible wavelength satellite data is absent during the long winter and it provides little contrast between the ice covered portions of the ocean and clouds during the summer. Infrared retrievals are hampered by intense low level temperature inversions which make it difficult to assign altitudes and open leads in the ice which make it difficult to specify the surface contribution to the observed radiance. Cloud fraction data from the HSRL in Eureka will provide an important source of validation for satellite climatologies.

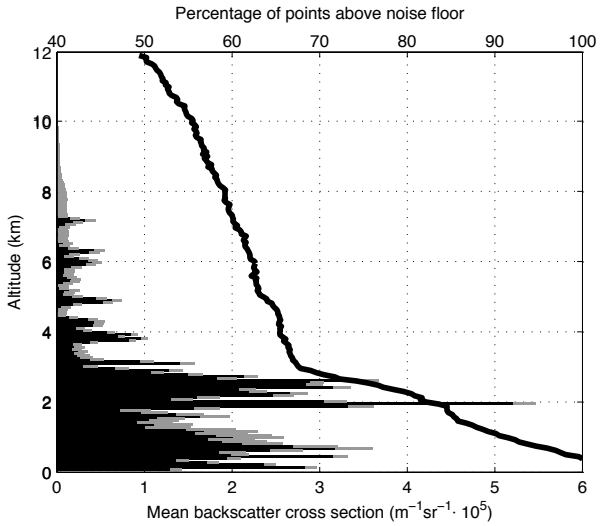

Figure 3. Monthly mean particulate backscatter cross section vs altitude for water (black) and ice (grey) and the percentage of lidar data points above the noise floor(black line). Data is from August of 2005 in Eureka.

Cloud climatologies often described cloud cover in terms of cloud fraction without specifying the threshold which distinguishes between cloudy and clear conditions. Figure 2 shows that cloud fraction is strong function of this threshold. Here we plot the fraction of the lidar profiles encountering a cloud as function of altitude above the lidar for the month of September, 2005 at Eureka. A profile is defined as cloudy when a threshold optical depth is reached. Separate curves are plotted for different thresholds. At 12 km, which is above all significant clouds at this location, the cloud fraction increases from 32% to 52% when the cloud threshold is decreased from optical depth 2 to optical depth 0.1.

Figure 3 shows the vertical variation in the monthly mean backscatter cross section for August 2005 at Eureka. Notice that low altitude water clouds and water fogs provide most of the optical depth with relatively small contributions from ice crystals. Higher altitudes are often obscured by low clouds.

Figure 4 shows the cloud fraction vs altitude and optical depth threshold for March 2006 in Eureka. The fractional cloudiness is much smaller than for August. The mean backscatter data for March (Fig. 5) shows a dramatic shift in cloud type relative to the August. With March surface temperatures often near $-40°$ C most of the scattering is due to ice crystals and often occurs in the form of ice fog.

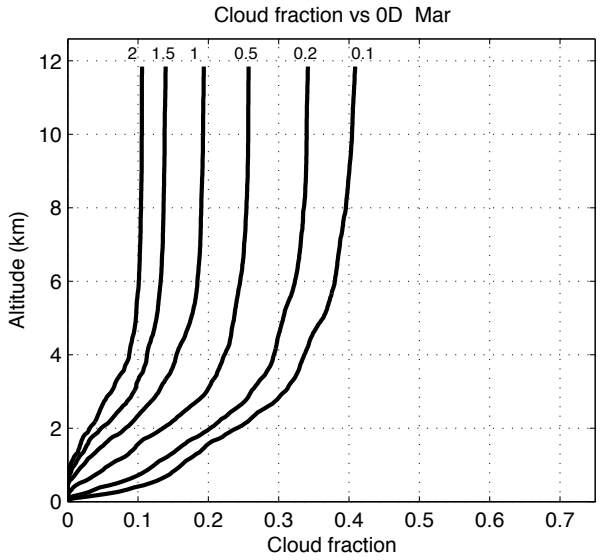

Figure 4. Cloud fraction as a function of altitude for March 2006 in Eureka. Curves show the fraction of the time that the atmosphere is clear up to a given altitude. Separate curves show the effect of changing the optical depth threshold that defines a cloud.

Figure 6 shows the distribution of backscatter phase function values observed in ice clouds and ice precipitation during March of 2006 in Eureka. Ice crystals were selected by considering only those points where the lidar depolarization was greater than 25%. In order to reject points which were contaminated by noise, only points with a lidar signal-to-noise ratio of at least 5 and with a backscatter cross section greater than 10^{-5} $\mathrm{m}^{-1}\mathrm{sr}^{-1}$ were included. Data points below 1 km were also excluded to minimize errors in the measured scattering cross section caused by uncertainties in the lidar overlap correction. This result from the Arctic, showing a distribution that is sharply peaked at a value of $P(180)/4\pi = .036$ is nearly identical to the distribution measured over Madison, WI [8; 9]. This information will be useful in analyzing data from satellite borne lidars.

The utility of combining radar and lidar data is illustrated in Figure 7. Radar measured Doppler velocities are shown as a function of the lidar-radar derived effective diameter. Data has been combined into 60 meter altitude and 180 second time averages for August 2005 at Eureka. All points meeting a signal-noise-threshold with a backscatter cross section greater than 10^{-6} $\mathrm{m}^{-1}\mathrm{sr}^{-1}$ were used to create this contour plot. This lidar-radar size retrieval assumed solid ice spheres and a gamma distribution of particle sizes. The concentration of points centered on zero Doppler velocity with diameters less than 30 microns is readily identified with water clouds when the figure is re-plotted excluding points with depolarization $< 20\%$. A 20% depolarization threshold also eliminates points in the region of 100 micron effective diameter and 1 m/sec fall velocities along with the small peak evident near 250 microns and 1.1 m/sec. These are

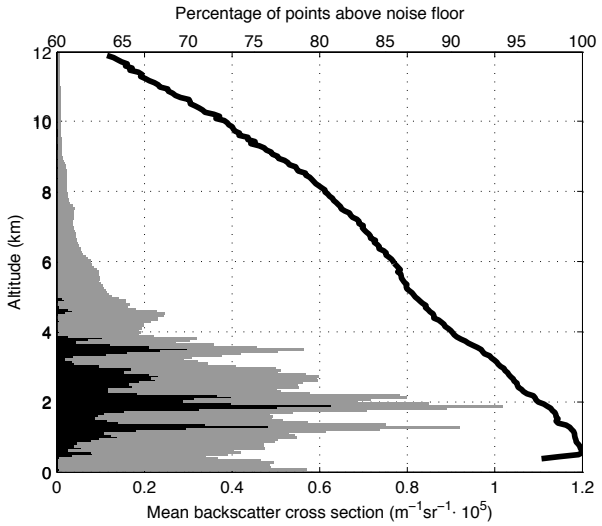

Figure 5. Monthly mean backscatter cross section for March 2006 in Eureka. Water contribution (black bars) and ice contribution (grey bars) with the black line showing the percentage of points above the noise floor.

associated with regions of high radar backscatter and are easily identified with periods of rain and drizzle that occurred on between Aug 19^{th} and 23^{th}. Variations in ice crystal shape pose a difficult problem for nearly all attempts to remotely characterize ice clouds. Further, investigation of particle fall velocity as a function of retrieved particle size may provide helpful constraints on the effects of particle shape.

Measurement of precipitation totals in the Arctic winter is difficult. Liquid water equivalents are small ($\sim$ 1 cm/month at Eureka). The precipitation falls as snow,

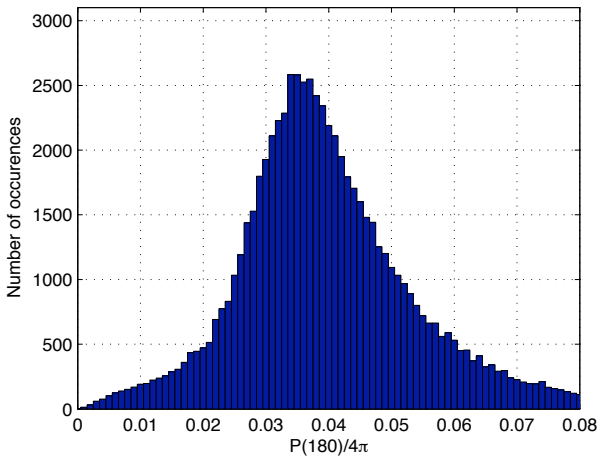

Figure 6. Backscatter phase function distribution for ice crystals during March, 2006. Data selected with depolarization $> 25\%$, altitude > 1 km, backscatter cross section $> 10^{-5}$ $\mathrm{m}^{-1}\mathrm{sr}^{-1}$ and a signal to noise ratio of > 5.

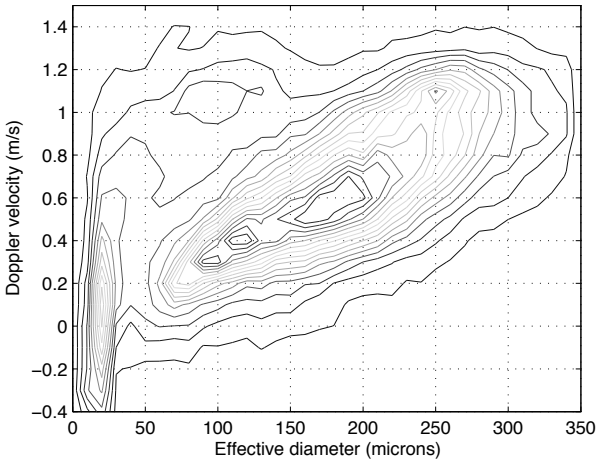

Figure 7. Fall velocity as a function of particle effective diameter for August 2005. Contours show the number of cloudy data points. Data points with signal-to-noise less than 2 are not plotted and a cloudy points are defined by backscatter cross section threshold $> 10^{-6}$ m^{-1}sr^{-1}.

Individual snow events may contribute only millimeters of accumulation. Wind affects the collection efficiency of snow gauges. Blowing snow is hard to distinguish from precipitation. Furthermore, drifting, small accumulations, cold and darkness make transect sampling difficult. The combination of lidar and radar offers another method of precipitation measurement. Figure 8 shows the product of the lidar-radar derived liquid water content and the radar Doppler velocity (lower line). The integral of this product (upper line) is the water equivalent total precipitation. Station records show the water equivalent precipitation provided by the snowfall on the 4^{th} and 5^{th} of Jan to be 3.3 mm, on the 7^{th} 0.2 mm, 2.8 mm on the 9^{th} and 0.2 mm on the 18^{th} (which was incorrectly reported as rain). All other days are listed as providing a trace of precipitation even though the radar and lidar show conclusively that many of these days provided no precipitation. The lidar-radar retrieval shows 20 mm compared to a 6.5 mm of water equivalent precipitation reported by the Eureka weather station. It is not surprising that the lidar-radar value is larger than the station value because the Doppler velocity used is the radar weighted fall velocity which is biased towards the fall velocity of the largest particles. Thus, this precipitation estimate assumes that all of the water mass is falling with the speed of the largest particles. Correcting for this bias requires assumptions about the ice crystal habit. However, in view of the conventional measurement difficulties, it appears useful to refine this approach in an attempt to improved Arctic precipitation measurements.

ACKNOWLEDGMENTS

This research was supported by National Science Foundation Grant OPP-9910304, NOAA agreement NA07EC0676 , and DOE Grant DE-FG02-06ER64187.

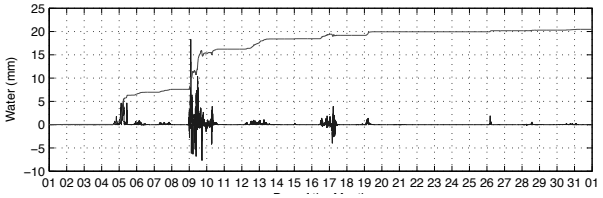

Figure 8. January, 2006 precipitation record derived from lidar-radar liquid water measurement and radar fall velocity measured 250 meters above the surface. The lower line shows the product of liquid water equivalent and Doppler velocity in gr m^{-2}sec^{-1}. This shows positive and negative excurssions due to atmospheric turbulence. The upper line shows the integral of this product, the total precipitation, in millimeters of water.

REFERENCES

[1] Knuteson, R. O., H. E. Revecomb, R. A. Best, N. C. Ciganovich, G. Dedecker, T. P. Dirkx, S. C. Ellington, W. F. Feltz, R. K. Garcia, H. B. Howell, W. Smith, J. f. Short and D. C. Tobin. Atmospheric Emitted Radiance Interferometer. *J. Atmos. Oceanic Technol.* 21(12), pp 1763-1776: 2004.

[2] Eloranta, E. W. High Spectral Resolution Lidar. *in Lidar: Range-Resolved Optical Remote Sensing of the Atmosphere*, Edited by C. Weitkamp, Springer-Verlag, New-York, 2005, 455p.

[3] Moran, K. P., B. E. Martner, M. J. Post, R. A. Kropfli, D. C. Welsh and K. B. Widener. An unattended cloud-profiling radar for use in climate research. *Bull. Amer. Meteor. Soc.* 79, 443-455, 1998.

[4] Donovan, D. P. and A. C. A. P. van Lammeren. Cloud effective particle size and water content profile retrievals using combined lidar and radar observations 1. Theory and examples. *J. Geophy. Res.* 106(D21), 27425-27448, 2001.

[5] Intrieri, J. M.,M. D. Shupe, T. Uttal, B. J. McCarty An annual cycle of Arctic cloud characteristics observed by radar and lidar at SHEBA. *J. Geophys. Res. (C Oceans)*, 107: 2002.

[6] Razenkov, I. A., E. W. Eloranta, J. P. Hedrick, R. E. Holz, R. E. Kuehn, and J. P. Garcia. A High Spectral Resolution Lidar Designed for Unattended Operation in the Arctic. *Proc. ILRC21, 57-60, 2002*

[7] Pirronen, P. A high spectral resolution lidar based on an iodine absorption filter Ph.D. thesis, Univ. of Joensuu, Joensuu, Finland, pp 113, 1994.

[8] Eloranta, E. W.,R. E. Kuehn, and R. E. Holz Measurements of backscatter phase function and depolarization in cirrus clouds made with the University of Wisconsin High Spectral Resolution Lidar. *Proc. ILRC20, 57-60, 2000* 255-257.

[9] R. E. Holz Measurement cirrus backscatter phase functions using a high spectral resolution lidar. University of Wisconsin-Madison MS Thesis, 2002, 67p.